Western and Central Tropical Pacific Rainfall Response to Climate Change: Sensitivity to Projected Sea Surface Temperature Patterns

C. DUTHEIL,[a] M. LENGAIGNE,[b] J. VIALARD,[c] S. JULLIEN,[d] AND C. MENKES[e]

[a] *Department of Physical Oceanography and Instrumentation, Leibniz Institute for Baltic Sea Research Warnemünde, Rostock, Germany*
[b] *MARBEC, University of Montpellier, CNRS, IFREMER, IRD, Sète, France*
[c] *LOCEAN-IPSL, Sorbonne Université, CNRS, IRD, MNHN, Paris, France*
[d] *ENTROPIE, IRD, Univ. de la Nouvelle Calédonie, Univ. de la Réunion, CNRS, Ifremer, Nouméa, Nouvelle-Calédonie*
[e] *IFREMER, University of Brest, CNRS, IRD, Laboratoire d'Océanographie Physique et Spatiale (LOPS), IUEM, Plouzané, France*

(Manuscript received 28 January 2022, in final form 21 April 2022)

ABSTRACT: Rainfall projections from the Coupled Model Intercomparison Project (CMIP) models are strongly tied to projected sea surface temperature (SST) spatial patterns through the "warmer-gets-wetter" mechanism. While these models consistently project an enhanced equatorial warming, they, however, indicate much more uncertain changes in zonal SST gradients. That translates into large uncertainties on rainfall projections. Here, we force an atmospheric model with synthetic SSTs whose zonal SST gradient changes span the range of CMIP5 uncertainties in the presence and in the absence of the robust equatorially enhanced warming. Our results confirm that projected rainfall changes are dominated by the effect of circulation changes, which are tied to SST through the "warmer-gets-wetter" mechanism. We show that SPCZ rainfall changes are entirely driven by the uncertain zonal SST gradient changes. The western equatorial Pacific rainfall increase is largely controlled by the robust enhanced equatorial warming for modest zonal SST gradient changes. However, for larger values, the effect of the zonal SST gradient change on rainfall projections becomes dominant due to nonlinear interactions with the enhanced equatorial warming. Overall, our study demonstrates that uncertainties in the zonal SST gradient changes strongly contribute to uncertainties in rainfall projections over both the South Pacific convergence zone and western equatorial Pacific. It is thus critical to reduce these uncertainties to produce more robust precipitation estimates.

KEYWORDS: Precipitation; Sea surface temperature; Climate change; Hydrologic cycle; Climate models; Regional models

1. Introduction

The rainfall response to anthropogenic climate change has major implications for the future of many Pacific island nations because it impacts many sectors of human activities including water resources, agriculture, infrastructures, and human health (McIver et al. 2016). This is particularly the case for the tropical western Pacific, where many countries consist of low-lying atolls, with heavy reliance on rain-fed agriculture due low water storage capacity, and groundwater that is exposed to pollution from sewage systems and agricultural activities (Duncan 2012; Falkland 2002). Providing reliable island-specific rainfall projections is thus necessary for regional adaptation planning. The main rainfall providers for tropical Pacific islands are the intertropical convergence zone (ITCZ) north of the equator and the South Pacific convergence zone (SPCZ) in the South Pacific (blue contours in Fig. 1a). The ITCZ and SPCZ are themselves strongly tied to the sea surface temperature (SST) distribution, as both develop for SSTs above 27°–28°C in the present-day climate (e.g., Graham and Barnett 1987).

Earth System Models (ESMs) gathered in the Coupled Model Intercomparison Project (CMIP, Taylor et al. 2012) are widely used for issuing future climate projections. As shown on Fig. 1a, these models consistently project an increase of climatological rainfall over the equatorial Pacific (Grose et al. 2014). Off the equator, rainfall projections are far less robust, especially under both the ITCZ (Byrne et al. 2018) and the SPCZ (Brown et al. 2020). Thus, there is a need to better understand the reasons behind these rainfall projections uncertainties.

The mechanisms leading to those rainfall changes are strongly tied to the projected SST changes through two distinct mechanisms. The first is "thermodynamical." A uniform surface ocean warming indeed results in a higher humidity loading due to the Clausius–Clapeyron equation. In the absence of circulation changes, this yields more rainfall in regions of surface convergence such as the ITCZ and SPCZ and less rainfall in regions of surface divergence. This mechanism associated with the effect of the present-day circulation on moisture changes is known as the "wet-gets-wetter paradigm" (e.g., Held and Soden 2006). This mechanism however usually yields smaller rainfall changes than those associated with changes in atmospheric circulation (Chadwick et al. 2013; Xie et al. 2010). Such circulation changes are strongly tied to SST changes. Fast atmospheric waves indeed homogenize the upper tropospheric warming in the tropics, which is equilibrated with the mean surface warming through moist adiabats. Atmospheric stability hence decreases in regions where SST warms more than the tropical mean, and increases in regions where it warms less (Johnson and Xie 2010). The SST minus its tropical mean or "relative SST" is a thus reasonable proxy for future atmospheric stability changes, with a projected rainfall increase in regions where the SST warms most: this is the "warmer-gets-wetter" paradigm (e.g., Xie et al. 2010).

As a result, uncertainties in projected regional SST patterns are a major source of uncertainties in future rainfall projections

Corresponding author: Cyril Dutheil, cyril.dutheil@io-warnemuende.de

DOI: 10.1175/JCLI-D-22-0062.1

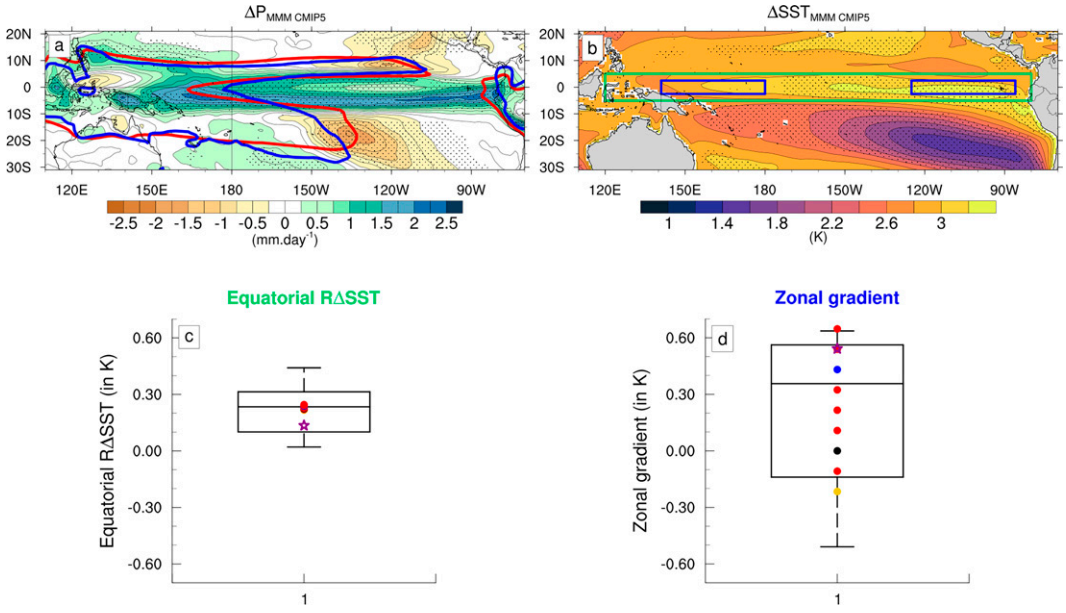

FIG. 1. DJF changes in (a) precipitation (in mm day^{-1}) and (b) SST (in K) projected by CMIP5 multimodel mean (MMM) between the future (2080–2100) and historical (1989–2009) periods under RCP8.5 scenario. Stippling in (a) and (b) indicate regions where more than 75% of CMIP5 models agree on the sign of precipitation changes and relative SST changes (RΔSST, defined as SST changes minus their tropical mean), respectively. Blue and red contours indicate observed (GPCP) and CMIP5 MMM rainfall reaching 5 mm day^{-1} over 1989–2009, respectively. Boxplots representing the CMIP5 distribution of (c) the equatorial relative SST change computed as the average of RΔSST in the green box domain in (b) (5°S–5°N, 120°E–80°W) and (d) the SST change zonal gradient, computed as the difference between the two blue boxes in (b) (note that the mean east-minus-west SST gradient at the equator is negative, so that a negative SST gradient anomaly indicates a strengthening of the east-minus-west SST gradient). The whiskers represent the 10th and 90th percentiles and the outliers are not represented. The colored dots represent values from the ABSW simulations ($\alpha = 2$ in blue; $\alpha = 0$ in black; $\alpha = -1$ in yellow, others α values in red, with 0.5 increment). The purple star represents the CMIP5 MMM, corrected using the method of Li et al. (2016) (see text for more details).

(Ma and Xie 2013; Xie et al. 2015). This is particularly the case in the SPCZ region, where the wet-gets-wetter mechanism tends to increase rainfall but is strongly offset by circulation changes associated with the warmer-gets-wetter mechanism (Brown et al. 2020; Widlansky et al. 2013).

As shown on Fig. 1b, CMIP5 models on average project an enhanced equatorial Pacific warming relative to off-equatorial regions. This enhanced equatorial warming has been related to a reduced evaporative damping at the equator (e.g., Liu et al. 2005; Xie et al. 2010), with some contribution from reduced ocean dynamical cooling induced by the Walker circulation slowdown (e.g., DiNezio et al. 2009). The multimodel model mean also projects an enhanced warming over the eastern equatorial Pacific compared to the western equatorial Pacific, leading to a reduction of the equatorial west–east SST gradient (Fig. 1b). This warming of the cold tongue has been attributed to a positive feedback loop between evaporative cooling and the trade wind reduction (e.g., Xie et al. 2010), increased vertical ocean heat transport arising from enhanced near-surface stratification in the cold tongue (DiNezio et al. 2009) and a limitation of the warming over the west Pacific by cloud feedbacks (e.g., Ramanathan and Collins 1991).

The enhanced equatorial warming is very robust across models (Fig. 1c), with only three CMIP5 models out of 31 projecting a relative equatorial SST cooling. On the other hand, the projected weakening of the zonal SST gradient is far less robust (Fig. 1d; Coats and Karnauskas 2017), with one-third of the models projecting a strengthening of the zonal SST gradient. This inconsistency between ESMs projections result from a great spread of the future SST changes in the western equatorial Pacific, and to corresponding uncertainties in the future rainfall changes (e.g., Li et al. 2016). In addition, historical changes simulated by CMIP models do not match the observed trend over recent decades, which is characterized by an eastern equatorial Pacific cooling (i.e., a strengthening of the zonal equatorial SST gradient), casting some doubts on the reliability of CMIP projections (Cai et al. 2021; Power et al. 2021). While some studies suggest that this mismatch may be related to internal variability of the climate system (Chung et al. 2019; Coats and Karnauskas 2017; Watanabe et al. 2021), other studies argue that ESMs systematic biases may lead to erroneous projections of SST patterns in the equatorial Pacific (e.g., Cai et al. 2019; Luo et al. 2018; Seager et al. 2019).

ESMs indeed generally exhibit common biases over the tropical Pacific, including an equatorial cold tongue that is too intense and extends too far into the western Pacific (e.g., Li and Xie 2014), and a too-zonal SPCZ (e.g., Brown et al. 2020; Lin 2007; Samanta et al. 2019) and blue and red contours in Fig. 1a). Several studies highlighted a statistical relationship between the intensity of the cold tongue bias and the spatial pattern of the projected SST change (e.g., Li et al. 2015, 2016;

Ying et al. 2019). The underpinning physical mechanism for such results is that the cold bias is associated with 1) a too-weak negative cloud–SST feedback in the western Pacific and 2) a too-strong wind-upwelling dynamic feedback in the eastern Pacific. This leads to an overestimated warming in the western Pacific, and an underestimated warming in the central and eastern Pacific. These statistical relationships can be used to correct the pattern of projected SST changes (e.g., Li et al. 2016) through the so-called emergent constraint methods (Hall et al. 2019). Resulting bias-corrected SST changes display a weaker warming in the western Pacific and a stronger warming in the eastern Pacific, i.e., a stronger reduction in the equatorial zonal SST gradient as indicated by the purple star (the bias-corrected multimodel mean value) in Fig. 1d.

Complementary to those statistical analyses on CMIP models, sensitivity experiments with atmospheric models have been used to investigate how biases and uncertainties in the projected SST changes may affect rainfall projections in the tropical Pacific. Zhou and Xie (2015) demonstrated that present-day ESM SST biases result in an overestimation of the rainfall increase in the eastern Pacific just south of the equator, and an underestimation of the Walker circulation slowdown. Such modeling strategy however did not explore the effects of uncertainties in the ESM projected SST warming pattern. Recently, Dutheil et al. (2019) using Li et al.'s (2016) bias-correction strategy showed that the statistical corrections of SST warming patterns from CMIP5 models induced an additional drying of the SPCZ in the future in response to an increased circulation change. While this confirms that the projected SPCZ changes are strongly sensitive to changes in the SST pattern, this study only explored one possible way of correcting the SST projections, and not the full range of plausible SST pattern changes given the uncertainties of ESMs. There is thus a need to explore the influence of the SST warming pattern on rainfall projections more widely.

To explore the projected rainfall sensitivity to the projected SST pattern, we design here a series of sensitivity experiments. We performed a first set of regional atmospheric model simulations where the enhanced equatorial warming is kept constant but where the zonal structure of the SST pattern varies and covers the range of the CMIP5 projected SST changes depicted on Fig. 1d. An additional set of experiments where the zonal mean SST warming is suppressed allows investigating potential nonlinear interactions between the robust zonal-mean warming and the uncertain changes in the zonal SST gradient. A vertically integrated water budget is used to identify the main mechanisms that contribute to precipitation changes in all these experiments. Details about the regional model configuration and experimental designs are provided in section 2, the results in section 3 and a summary and discussion in section 4.

2. Methods

a. WRF configuration and control experiment

We use the same configuration of the Weather Research and Forecasting (WRF) Model version 3.9.1 as the one of Dutheil et al. (2019, 2020, 2021). This configuration covers the tropical Pacific region (26°N–42°S, 101°E–59°W) at 1° × 1° horizontal resolution with 32 vertical levels. The use of a regional configuration allows us to reduce the computation time and thus to perform a large number of sensitivity experiments. The physical parameterizations include Lin et al. (1983) microphysics scheme, the Community Atmosphere Model (Collins et al. 2004) for shortwave and longwave radiation, the University of Washington (UW) planetary boundary layer (Bretherton and Park 2009) with the Monin–Obukhov surface layer parameterization, and the Noah land surface model (Chen and Dudhia 2001). The parameterization of subgrid-scale convection is taken from the Zhang–McFarlane scheme (Zhang and McFarlane 1995).

Our control experiment (CTRL) for present-day conditions is run over the 1980–2016 period, with surface and lateral boundary conditions extracted from 6-h outputs of NCEP2 reanalysis, and a CO_2 concentration that is representative of present-day conditions (379 ppm). Such experiment has already been evaluated in Dutheil et al. (2019), and we hence only briefly validate the climatological present-day rainfall here. The CTRL simulation accurately captures the major climatological features in the southwest Pacific (Fig. 2). The SPCZ orientation is relatively close to observations, despite a slight underestimation of its slope (0.18°S/°E versus 0.23° and 0.24°S/°E in CPC Merged Analysis of Precipitation (CMAP; Xie and Arkin 1997) and Global Precipitation Climatology Project (GPCP; Adler et al. 2003) observations, respectively; Fig. 2a). Rainfall rates are also realistic despite a dry bias in the western equatorial Pacific and too much rainfall in the SPCZ core (Table 1). In addition, the bias relative to GPCP tends to be weaker than observational uncertainties estimated from the CMAP minus GPCP differences (Fig. 2). More details on the CTRL experiment evaluation can be found in Dutheil et al. (2019).

b. Experimental design

We computed the CMIP5 multimodel mean (MMM)-projected SST change (ΔSST) as the seasonal (for each month of the year) SST difference between the future (2080–2100) and historical (1989–2009) periods under RCP8.5 scenario.

We estimate the equatorially enhanced warming ΔSST_e (Fig. 3b) as the zonally averaged ΔSST, i.e., the average of ΔSST over all the Pacific oceanic grid points along each latitude. And thus the zonal SST gradient changes ΔSST_g is computed as follows:

$$\Delta SST_g(\alpha) = \alpha'(\Delta SST - \Delta SST_e), \quad (1)$$

with α varying from −1 to 3 in steps of 0.5 (Figs. 3e–h).

The corresponding values of the zonal gradients are indicated using colored dots on Fig. 1d: $\alpha = -1$ samples the lower end of the CMIP5 zonal SST gradient changes distribution, showing a slight increase of the zonal equatorial SST gradient relative to present-day values, while $\alpha = 3$ corresponds to the CMIP5 models with the largest reduction of the zonal SST gradient. This method is similar to that of van der Wiel et al. (2016), but it is applied to SST changes instead of the present-day climatological SST.

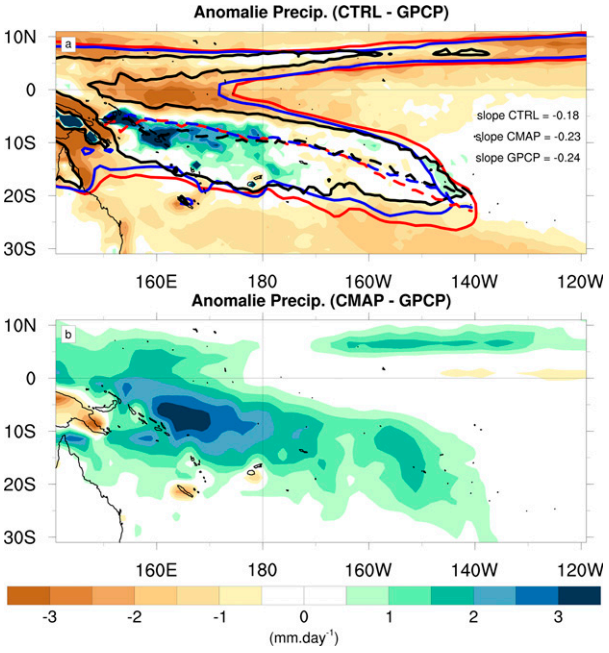

FIG. 2. Precipitation anomalies (shading; in mm day^{-1}) for DJF climatology calculated as the difference between (a) CTRL and GPCP observations and (b) CMAP and GPCP observations. Dashed and thick lines in (a) represent the mean position of SPCZ and the 6 mm day^{-1} isopleth, respectively, for CMAP (blue), CTRL (black), and GPCP (red). The slope (°E/°N) of the SPCZ mean position for each dataset is also indicated in (a).

We perform two sets of nine experiments over the 1980–2016 period. Those experiments are summarized in Table 2. The first set is referred to as RELW for relative warming. This set only differs from the CTRL experiment through the surface boundary condition: the variable $\Delta SST_g(\alpha)$ SST change (Figs. 3e–h) is added to the CTRL SST (note that the $\alpha = 0$ RELW experiment corresponds to the CTRL experiment). This introduces some inconsistency between the SST and the lateral boundary conditions near the domain boundaries, but we did perform an extra experiment that shows that this does not influence our results (see discussion in the appendix).

The second set of experiments is referred to as ABSW for absolute warming. In this set $\Delta SST_e + \Delta SST_g(\alpha)$ (Figs. 3a–d) is added to the CTRL SST (note that the $\alpha = 0$ ABSW experiment corresponds to an experiment where only the enhanced equatorial warming is applied). Since this set is characterized by a mean warming, typical of the climate change signals, changes in lateral boundary conditions from CMIP5 (computed as they were for the MMM SST change) are added to the NCEP2 present-day boundary conditions (see Table 3 for fields used). The CO_2 forcing is set to a value representative of the future period (2080–2100) for the RCP8.5 scenario (845 ppm).

c. Decomposition of precipitation changes

Precipitation changes in the ABSW experiment are obtained as follows:

TABLE 1. CTRL and MMM of CMIP5 models precipitation bias (in mm day^{-1}) relative to CMAP and GPCP observations in the western equatorial region (5°S–5°N, 140°–180°E) and the SPCZ region (5°S–5°N, 160°–240°E).

Precipitation bias (mm day^{-1})	Western equatorial region (5°S–5°N, 140°–180°E)	SPCZ region (20°S–5°N, 160°–240°E)
CTRL − CMAP	−3.1	−0.9
CMIP5 MMM − CMAP	−1.6	0.4
CTRL − GPCP	−1.7	0.1
CMIP5 MMM − GPCP	−0.3	1.6

$$\Delta P(\alpha) = P_{\mathrm{ABSW},\alpha} - P_{\mathrm{CTRL}}. \quad (2)$$

Those precipitation changes include three components:

$$\Delta P(\alpha) = \Delta P_e + \Delta P_g(\alpha) + \Delta P_n(\alpha), \quad (3)$$

where ΔP_e is the precipitation change in response to the enhanced equatorial warming ΔSST_e, $\Delta P_g(\alpha)$ precipitation change in response to the variable zonal SST gradient $\Delta SST_g(\alpha)$, and $\Delta P_n(\alpha)$ the potential nonlinear interaction between the two.

The precipitation response to the enhanced equatorial warming ΔSST_e that forces the ABSW, ($\alpha = 0$) experiment is obtained as follows:

$$\Delta P_e = P_{\mathrm{ABSW},(\alpha=0)} - P_{\mathrm{CTRL}}. \quad (4)$$

The precipitation response to the zonal SST gradient changes $\Delta SST_g(\alpha)$ that forces the RELW,(α) experiment are obtained as follows:

$$\Delta P_g(\alpha) = P_{\mathrm{RELW},\alpha} - P_{\mathrm{CTRL}}. \quad (5)$$

The potential nonlinear interactions between the enhanced equatorial warming and the changes in zonal SST gradient are obtained as the Eq. (1) residual or equivalently as follows:

$$\Delta P_n(\alpha) = P_{\mathrm{ABSW},\alpha} - P_{\mathrm{ABSW},(\alpha=0)} - \Delta P_g(\alpha). \quad (6)$$

This approach can be applied to any variable, to specifically isolate its response to ΔSST_e, $\Delta SST_g(\alpha)$, and their potential nonlinear interactions.

d. Divergence of moisture flux

Moisture flux divergence is a good approximation of the large-scale, low-frequency tropical precipitation (e.g., Neelin and Held 1987; Seager et al. 2010). We thus decompose the precipitation changes in the ABSW,α experiment into three terms, as in Chung et al. (2014):

$$\Delta P(\alpha) = \Delta \mathrm{DYN}(\alpha) + \Delta \mathrm{THE}(\alpha) + \Delta \mathrm{MIX}(\alpha). \quad (7)$$

The dynamical term (labeled DYN) is associated with the effect of circulation changes $\Delta\mathbf{u}(\alpha)$ on the present-day humidity q, i.e., to the "warmer-gets-wetter" mechanism discussed in the introduction:

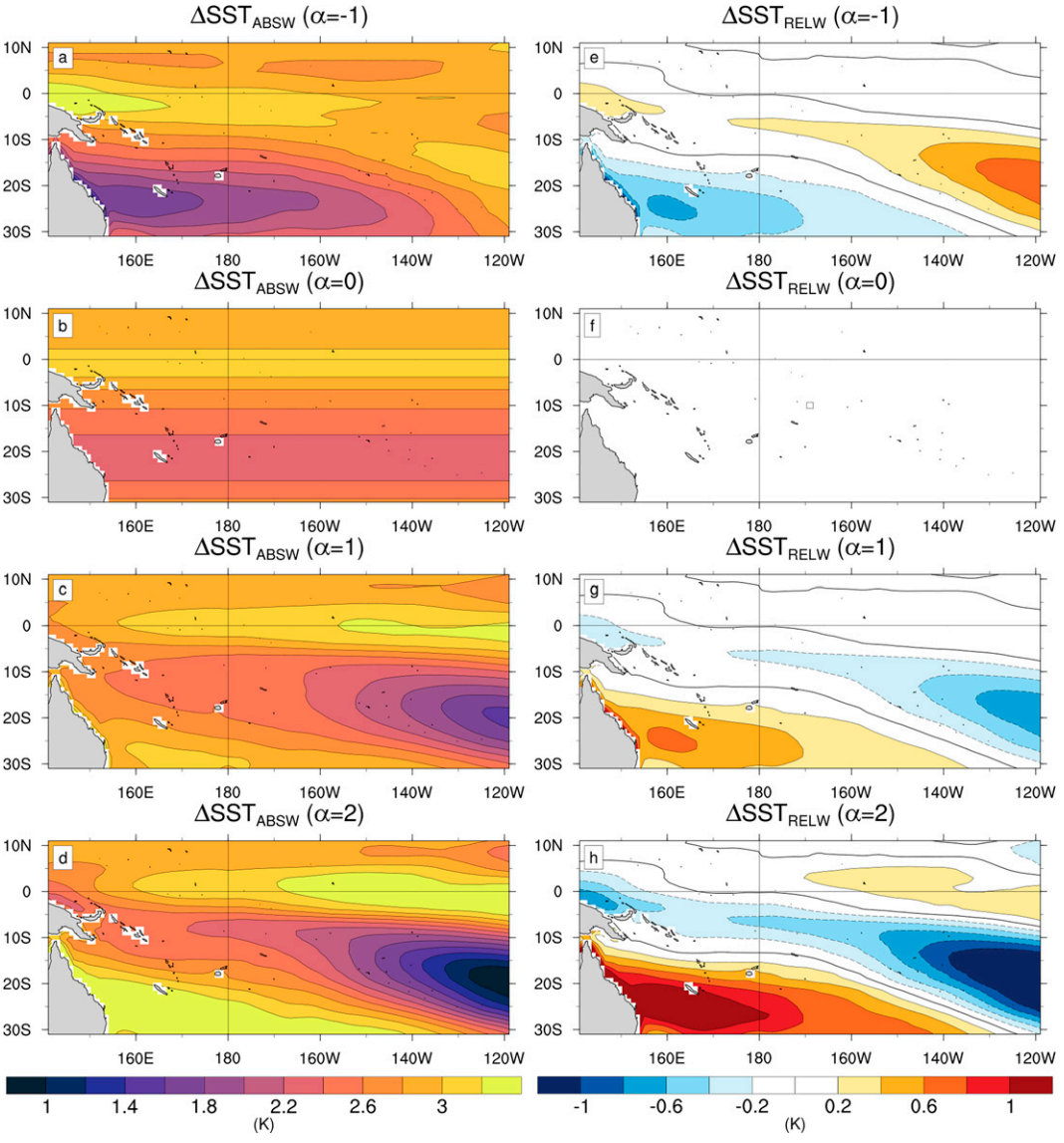

FIG. 3. December–February (DJF) average SST changes (in K) applied in the (a)–(d) ABSW and (e)–(h) RELW experiments, for different values of the α parameter. The RELW ($\alpha = 0$) experiment has no SST change applied and is used as a historical reference to compute projected changes in other experiments.

$$\Delta\mathrm{DYN}(\alpha) = \frac{-1}{\rho g}\int_0^{P_s} \boldsymbol{\nabla} \cdot [\Delta\mathbf{u}(\alpha)\overline{q}]dp, \qquad (8)$$

where ρ is the air density, g is the gravity acceleration, P_s is the surface pressure, $\mathbf{u}$ is the horizontal wind vector, q is the specific humidity, the overbar denotes the present-day simulation climatology, and Δ the future minus present simulation climatology.

The thermodynamical term (labeled THE) is associated with the effect of moisture changes $\Delta q(\alpha)$ on the present-day circulation $\mathbf{u}$, i.e., to the "wet-gets-wetter" mechanism:

TABLE 2. List and description of experiments.

Expt	Absolute warming (ABSW)	Relative warming (RELW)
CO_2 forcing	845 ppm	379 ppm
Boundary conditions	NCEP2 + [CMIP5 MMM (2080–2100) − CMIP5 MMM (1989–2009)]	NCEP2
SST forcing	$\mathrm{SST}_{\mathrm{CTRL}} + \Delta\mathrm{SST}_e + \alpha \times \Delta\mathrm{SST}_g$	$\mathrm{SST}_{\mathrm{CTRL}} + \alpha \times \Delta\mathrm{SST}_g$
Asymmetry strength α	[−1:0,5:3]	[−1:0,5:3], $\alpha = 0$ = CTRL

TABLE 3. List of variables concerned by the delta methodology.

Variables	Variable dimensions	Units
Specific humidity	3D	kg kg^{-1}
Temperature	3D	K
U component of wind	3D	m s^{-1}
V component of wind	3D	m s^{-1}
Geopotential height	3D	m
Relative humidity at 2 m	2D	Percent
U component of wind at 10 m	2D	m s^{-1}
V component of wind at 10 m	2D	m s^{-1}
Temperature of surface at 2 m	2D	K
Pressure at surface	2D	Pa
SST/land skin temperature at the surface	2D	K
Sea level pressure	2D	Pa

$$\Delta\mathrm{THE}(\alpha) = \frac{-1}{\rho g}\int_0^{P_s} \nabla \cdot [\overline{\mathbf{u}}\Delta q(\alpha)]dp. \quad (9)$$

The mixed term (labeled MIX) is associated with the effect of circulation changes $\Delta\mathbf{u}(\alpha)$ on moisture changes $\Delta q\ (\alpha)$:

$$\Delta\mathrm{MIX}(\alpha) = \frac{-1}{\rho g}\int_0^{P_s} \nabla \cdot [\Delta\mathbf{u}(\alpha)\Delta q(\alpha)]dp. \quad (10)$$

The decomposition of the precipitation changes in section 2c into a response to $\Delta\mathrm{SST}_e$, $\Delta\mathrm{SST}_g(\alpha)$, and nonlinear effects can be applied to the various terms of Eq. (6). For linear terms like DYN and THE, the resulting expression is straightforward [e.g., $\Delta\mathrm{DYN}_e$ involves $\nabla \cdot (\Delta\mathbf{u}_e)\overline{q}$, and $\Delta\mathrm{DYN}_g$ involves $\nabla \cdot (\Delta\mathbf{u}_g)\overline{q}$, i.e., $\Delta\mathrm{DYN}_e$ only involves circulation changes in response to $\Delta\mathrm{SST}_e$]. It is only for the MIX term that cross-products between the various components appear [e.g., $\nabla \cdot (\Delta\mathbf{u}_e)\Delta q_g(\alpha)$, a term that involves both the response to the robust $\Delta\mathrm{SST}_e$ and to $\Delta\mathrm{SST}_g\ (\alpha)$.

3. Results

In section 3a, we first discuss climatological precipitation changes in response to the robust enhanced equatorial warming in CMIP models, focusing on austral summer [December–February (DJF) average] because it corresponds to the season with the maximum extension of the SPCZ. The effect of the uncertain zonal SST change in the absence of a zonal-mean warming is then assessed in section 3b. We finally investigate nonlinear interactions between the uncertain part of the SST change and the more robust equatorially enhanced warming in section 3c.

a. *Precipitation changes due to the robust equatorial enhanced warming ΔSST_e*

Figure 4 displays DJF rainfall, surface wind, and moisture divergence changes due to the equatorial warming $\Delta\mathrm{SST}_e$, which is displayed on Fig. 3b. $\Delta\mathrm{SST}_e$ drives a dipolar rainfall response, with a wetter equator and pronounced rainfall increase in the western Pacific near Papua New Guinea and a drying to the south. This pattern captures two aspects of the CMIP5 robust response to climate change (Fig. 1a): the enhanced equatorial precipitation and drying in the southeastern tropical Pacific, suggesting that these aspects are partly related to the enhanced equatorial warming.

Moisture transport divergence changes (contours on Fig. 4a) match precipitation changes very well (spatial pattern correlation of 0.85), justifying the use of the moisture divergence budget to understand these rainfall changes. The mixed term is a minor contributor to the budget (cf. Figs. 4a,d). The thermodynamical term is also weak (Figs. 4a,c), and resembles the precipitation climatology (spatial pattern correlation of 0.75), as expected from the wet-gets-wetter mechanism. The dominant term is the dynamical term: there is a 0.84 spatial pattern correlation between $\Delta\mathrm{DYN}_e$ (Fig. 4b) and ΔP_e (Fig. 4a). This indicates that circulation changes drive the rainfall in response to the enhanced equatorial warming. As underlined by previous studies, this circulation change is broadly consistent with the "warmer-gets-wetter" mechanism. The wind response in the Southern Hemisphere indeed converges toward the largest SST warming (Fig. 3b) in the equatorial band (Fig. 4b). This does not explain, however, why the rainfall increase is largest close to Papua New Guinea. Previous studies have noted that the positive convergence feedback (i.e., the fact that convergence anomalies strengthen rainfall changes due to moisture transport and that those rainfall changes reinforce the convergence anomaly through Matsuno–Gill dynamics) can only occur in high rainfall regions (e.g., Zebiak 1986). To account for that effect, previous studies have used rainfall changes proxies based on SST (Flannaghan et al. 2014; Fueglistaler et al. 2015; Sobel et al. 2002) or relative SST (Izumo et al. 2020) weighted by climatological rainfall. Contours on Fig. 4b indeed confirm that relative SST changes weighted by present-day rainfall matches reasonably well the dynamical term $\Delta\mathrm{DYN}_e$, especially for the enhanced rainfall change near Papua New Guinea. Overall, those analyses tend to support the warmer-gets-wetter mechanism invoked by previous studies: the enhanced equatorial warming drives anomalous convergence near the equator and anomalous divergence south of ~8°S, with a maximum rainfall increase in the far western Pacific where high present-day rainfall allow the positive convergence rainfall feedback to operate.

b. *Precipitation changes due to the uncertain zonal SST gradient change ΔSST_g*

The top panels in Fig. 5 display DJF precipitation, surface wind, and moisture divergence changes in response to $\Delta\mathrm{SST}_g$ for $\alpha = 2$ and $\alpha = -1$, respectively corresponding to a weakening and an enhancement of the zonal equatorial gradient (Figs. 1d, 3e,d). The $\Delta\mathrm{SST}_g(\alpha = 2)$ forcing yields a drying in the SPCZ region and more rainfall in the equatorial region (Fig. 5a), while the $\Delta\mathrm{SST}_g(\alpha = -1)$ experiment yields weaker opposite patterns (Fig. 5c). In both cases, the precipitation changes match very well the moisture divergence changes (contours in Figs. 5a–c), which are almost entirely explained by the dynamical effects (i.e., changes in wind divergence; Figs. 5b–d). The average rainfall response as a function of α at the equator and within the SPCZ shown in Figs. 5e and 5f confirms that rainfall changes in these two regions are entirely controlled by the dynamical term,

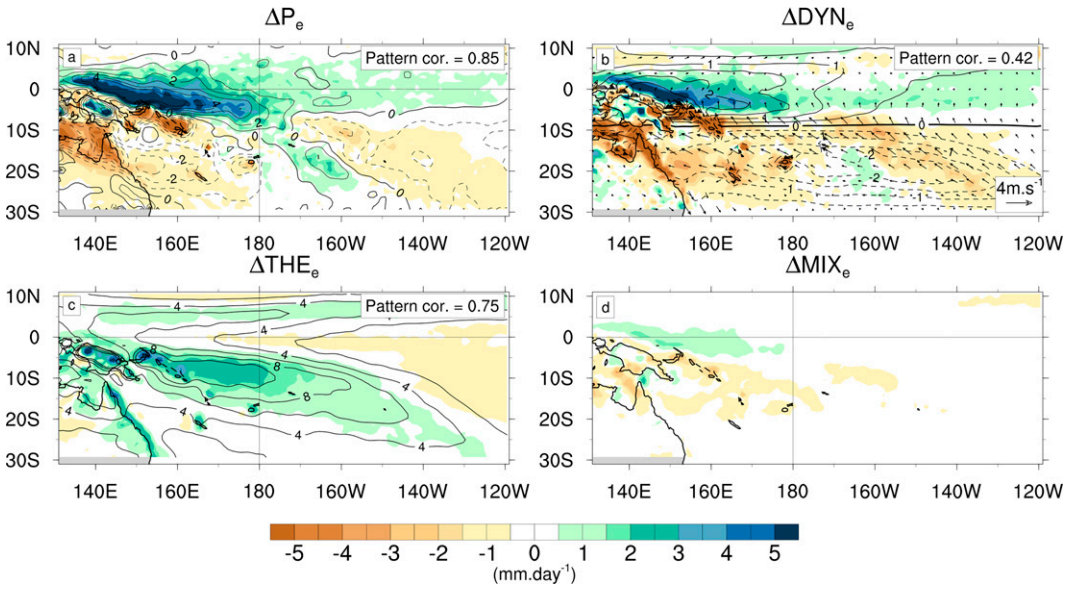

FIG. 4. Precipitation response to the enhanced equatorial warming from CMIP5. December–February (DJF) average (a) precipitation (shading; in mm day^{-1}) and moisture divergence (contours; in mm day^{-1}) changes for the ABSW ($\alpha = 0$) experiment that corresponds to the zonal-mean MMM projected CMIP5 SST change (Fig. 2b). Changes are estimated from the ABSW ($\alpha = 0$) minus the reference present-day experiment (RELW,$\alpha = 0$). The moisture divergence is further decomposed (see section 2d for details) into its (b) dynamical (circulation changes), (c) thermodynamical (humidity changes), and (d) mixed (term involving the circulation and humidity change) contributions. Vectors in (b) represent the surface wind changes (in m s^{-1}). The numbers in the upper-right corners indicate the pattern correlation between (a) the precipitation and the total convergence moisture changes, (b) the dynamical term and relative SST changes multiplied by the present-day climatological precipitation (contours), and (c) the thermodynamical term and climatological precipitation (contours).

which increases linearly with α. This indicates that ΔSST_g drives circulation changes that dominate the precipitation changes, both at the equator and under the SPCZ.

Let us now discuss what drives those circulation changes in response to ΔSST_g. As was the case for the response to ΔSST_e, changes in surface divergence tend to match those in relative SST weighted by present-day rainfall quite well (0.87 and 0.63 pattern correlation), in agreement with the warmer-gets-wetter mechanism. For instance for $\Delta SST_g(\alpha = 2)$, the relative cooling under the northern flank of the SPCZ produces near-surface divergence and drying, while the relative warming at the equator and south of 15°S produces near-surface convergence and more rainfall (Figs. 5a,b).

Overall, here we find that the precipitation response associated with the zonal SST gradient change ΔSST_g is also entirely driven by circulation changes and in general consistent with the warmer-gets-wetter mechanism. Experiments where the zonal equatorial gradient weakens yield more rainfall along the equator and less rainfall under the SPCZ (Figs. 5a,e,f), with the opposite signature in experiments where the gradient strengthens (Figs. 5c,e,f).

c. *Nonlinear interactions between the zonal-mean and zonally asymmetric warming*

The methodology described in section 2c allows isolating the precipitation response $\Delta P_n(\alpha)$ that arises from nonlinear interactions between responses to the equatorial warming ΔSST_e (Fig. 1c) and zonal gradient SST changes $\Delta SST_g(\alpha)$ (Fig. 1d). Figure 6a indicates that the nonlinear response also matches the moisture divergence changes very well (shading and contours on Fig. 6a).

Overall, this nonlinear response is dominated by the dynamical term, i.e., by the effect of the nonlinear circulation response $\Delta \mathbf{u}_n(\alpha)$ [$\Delta \mathbf{u}_n(\alpha) = \Delta \mathbf{u}_{tot}(\alpha) - \Delta \mathbf{u}_e - \Delta \mathbf{u}_g(\alpha)$] on the present-day humidity q (cf section 2d), with a weaker contribution from the MIX term and a negligible contribution from thermodynamical effects (Figs. 6a–d).

Let us focus on the equatorial region, where the nonlinear contribution to the rainfall change is largest (Figs. 6e,f): in this region the dynamical term explains about two third of the rainfall response and the MIX term only one-third. The MIX term corresponds to cross terms involving the circulation and humidity changes resulting from the enhanced equatorial warming, the SST gradient and the nonlinear changes. The fact that the dynamical term ΔDYN_n involving $\nabla \cdot (\Delta \mathbf{u}_n)\overline{q}$ terms dominates nonlinearities indicates that the circulation changes $\Delta \mathbf{u}_n$ themselves arise from a nonlinear process. We hypothesize that this nonlinear process is largely related to the convergence feedback described in Zebiak (1986). This process describes the mutual interaction between rainfall anomalies, which reinforce the circulation through Matsuno–Gill dynamics and convergence which reinforces rainfall through its effect on the vertically integrated water budget. Zebiak (1986) notes that this effect

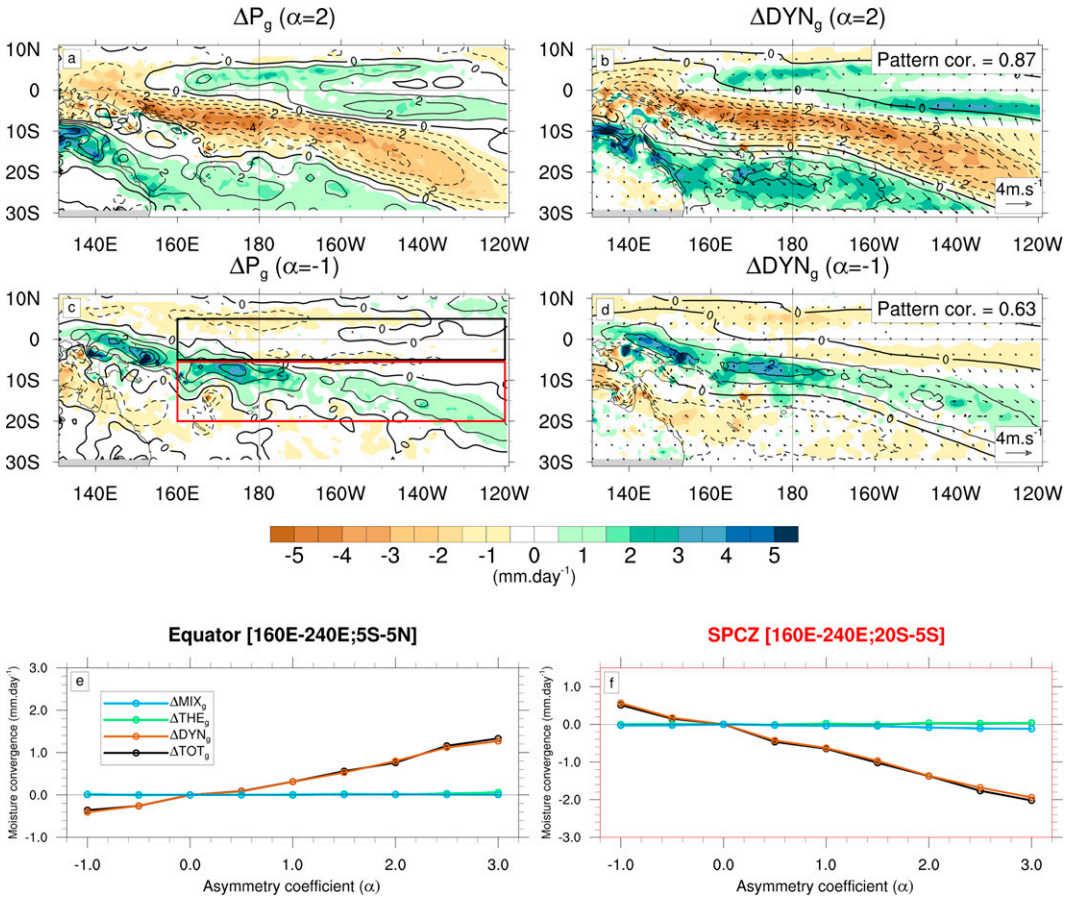

FIG. 5. Precipitation response to the zonal SST gradient change from CMIP5. December–February (DJF) average precipitation (shading; in mm day^{-1}) and moisture divergence (contours; in mm day^{-1}) changes for (a) the RELW ($\alpha = 2$) and (c) the RELW ($\alpha = -1$) experiments. Future changes are estimated as RELW ($\alpha = 2$ or $\alpha = -1$) minus the reference present-day experiment (RELW,$\alpha = 0$). (b),(d) As in (a) and (c), but for the dynamical (circulation changes) contribution to the moisture divergence change. Contours (solid for positive and dashed for negative) and vectors in (b) and (d) respectively represent the relative SST changes multiplied by the present-day climatological precipitation and the surface wind changes. The pattern correlation between the dynamical term and relative SST changes multiplied by the present-day climatological precipitation is indicated on the upper-right corner of (b) and (d). Average (e) equatorial box [black box in (c)] and (f) SPCZ box [red box in (c)] DJF moisture convergence change (black; in mm day^{-1}) as a function of the α coefficient. The brown, green, and blue lines respectively indicate the dynamical, thermodynamical, and mixed contributions to the total moisture convergence change.

can only operate in regions where the total wind field is convergent.

Figure 7a supports this hypothesis: the dynamical contribution associated with nonlinearities (and hence the nonlinear circulation change; brown line) is equal to zero for negative values of α, and only becomes positive for positive values in the equatorial region. This is because the present-day circulation is divergent on average in this region (black dashed line), and the equatorial warming ΔSST_e only is not sufficient to make it convergent ($\alpha = 0$ in black thick line; Fig. 7a). It is only in presence of SST gradient changes associated with $\alpha > 0$ that there is a shift to a convergent total circulation (black thick line) and that there is thus an extra convergence associated with nonlinear convergence feedback (brown line). Under the SPCZ, only the most extreme α value of 3 induces a shift to a divergent circulation (black thick line in Fig. 7b), explaining why there is no nonlinear interaction between the equatorially enhanced warming and zonal gradient change for most of the α range.

d. *Relative contribution of ΔSST_e, ΔSST_g, and their nonlinear interactions to the precipitation changes*

Figures 8a and 8b shows total rainfall changes two contrasting cases of the SST pattern changes: a strengthening ($\alpha = -1$, see Fig. 3a) and a weakening ($\alpha = 2$, see Fig. 3d) of the zonal SST gradient changes. These two cases are contrasted but do not even span the full range of zonal SST gradient changes in CMIP5 (Fig. 1d). Those uncertainties in the zonal SST

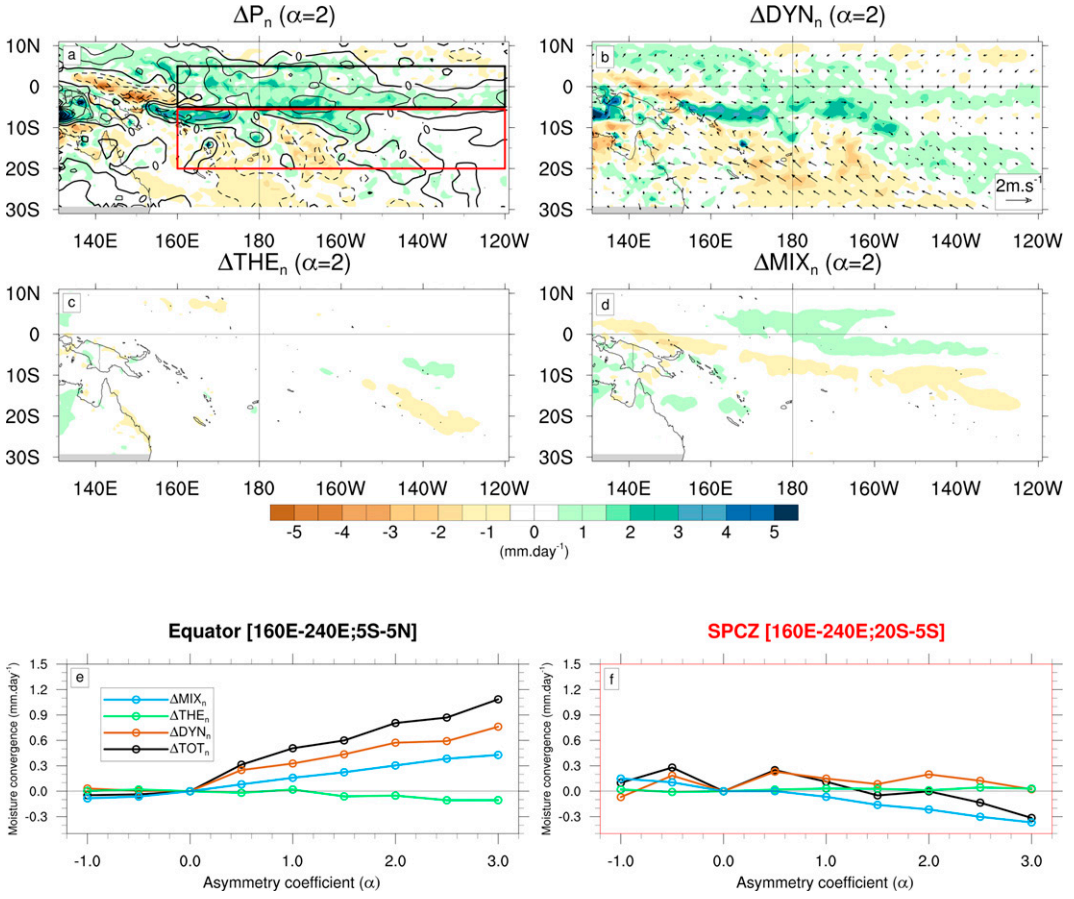

FIG. 6. Nonlinear precipitation response due to the interaction between the robust zonal-mean and uncertain zonally asymmetric projected SST change. (a) DJF ABSW minus RELW precipitation (shading; in mm day^{-1}) and moisture divergence (contours; in mm day^{-1}) changes for $\alpha = 2$. DJF ABSW minus RELW (b) dynamical contribution to the moisture convergence, with vectors indicating the ABSW minus RELW wind changes (c) thermodynamical contribution to the moisture convergence and (d) mixed contribution to the moisture convergence. Average DJF ABSW minus RELW moisture changes (black; in mm day^{-1}) as a function of α (e) in the equatorial box [black box in (a)] and (f) in the SPCZ box [red box in (a)]. The brown, green, and blue lines respectively indicate the dynamical, thermodynamical, and mixed contributions to the ABSW minus RELW moisture convergence change.

gradient changes result in large uncertainties on the projected rainfall change (Figs. 8a,b): the equatorial gradient strengthening case corresponds mostly to a strong rainfall increase in the far western Pacific, with no clear effects elsewhere, while the weakening case is associated with more widespread changes including a clear rainfall increase along the equator and drying under the SPCZ.

Figures 8c and 8d further summarizes contributions from the equatorial warming ΔP_e (red), from the zonal SST gradient changes $\Delta P_g(\alpha)$ (dark blue) and from nonlinear interactions

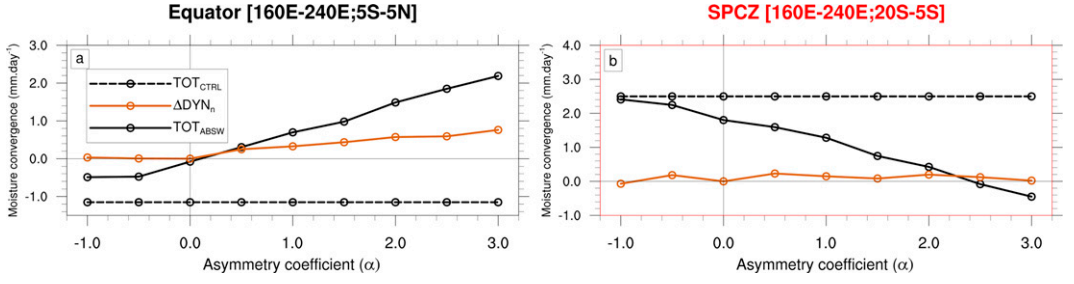

FIG. 7. Moisture convergence. Average DJF moisture convergence (in mm day^{-1}) in ABSW (black thick lines), CTRL (black dashed lines), and dynamical contributions to the ABSW minus RELW moisture convergence change (brown) as a function of α (a) in the equatorial box (black box in Fig. 5a) and (b) in the SPCZ box (red box in Fig. 5a).

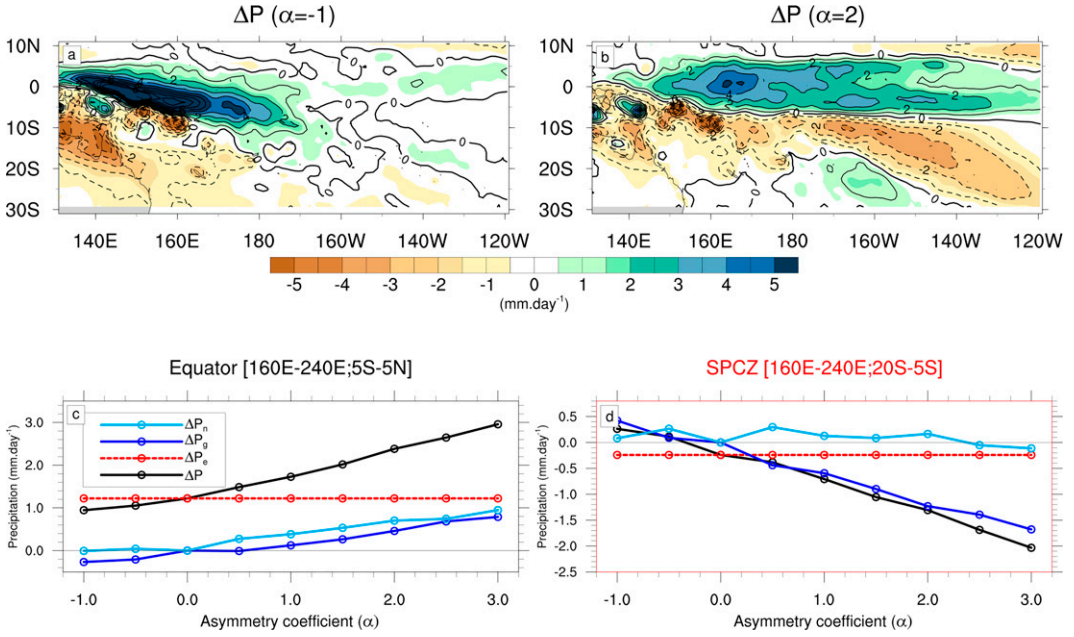

FIG. 8. Spatial pattern of precipitation changes (in mm day^{-1}) in the ABSW experiment for (a) $\alpha = -1$ and (b) $\alpha = 2$. (c) Average equatorial box and (d) SPCZ DJF precipitation changes (black; in mm day^{-1}) as a function of α, and their decomposition into contributions from the zonal-mean SST change (dashed red; ΔP_e), the SST change spatial pattern (dark blue; ΔP_g), and nonlinearities (light blue; ΔP_n).

between the equatorial warming and the zonal gradient changes $\Delta P_n(\alpha)$ (light blue) to rainfall changes $\Delta P(\alpha)$ (black) between the future climate and the present-day rainfall. In the SPCZ region, rainfall changes are largely driven by changes in the zonal SST gradient, with positive zonal SST gradient changes inducing a drying and a negative wetting. The enhanced equatorial warming in response to climate change (RCP8.5) contributes to a ~0.2–0.3 mm day^{-1} drying, a much smaller contribution than that of the zonal SST gradient changes. Finally, nonlinear interactions between the equatorial warming and zonal SST gradient changes can be neglected under the SPCZ. On the other hand, none of the three effects can be neglected in the equatorial region (5°S–5°N). The ~1 mm day^{-1} precipitation increase induced by the equatorial warming explains more than 50% of the total precipitation changes for $\alpha \leq 1.5$. The contribution of the zonal gradient and its nonlinear interaction with the equatorial warming contribute roughly equivalently, and dominate precipitation changes for $\alpha \geq 2$. For $\alpha = 3$, for instance, their combined contribution explain ~60% of total precipitation changes.

These results highlight that the uncertainties of zonal SST gradient changes $\Delta SST_g(\alpha)$ in CMIP5 models account for most of the future precipitation uncertainties in CMIP models through the warmer-gets-wetter mechanism. On the other hand, the uncertain zonal gradient change and its nonlinear interaction with the equatorial warming only dominate the equatorial rainfall changes for $\alpha \geq 2$, i.e. the robust enhanced equatorial warming tends to dominate the equatorial rainfall increase for $\alpha \leq 1.5$. This is a likely explanation of why future rainfall changes in CMIP are more robust along the equator than under the SPCZ (Fig. 1a). In the following section, we discuss the relevance of our results for CMIP5 more extensively.

4. Discussion: Relating our experiments to CMIP5 projected precipitation changes

The current paradigm to explain tropical precipitation changes in response to anthropogenic forcing is a competition between the "wet-gets-wetter" and "warmer-gets-wetter" mechanisms. In the SPCZ region, previous studies (e.g., Brown et al. 2013; Widlansky et al. 2013; Dutheil et al. 2019; Brown et al. 2020) have shown that these two effects tend to oppose each other, the SPCZ being moistened by the "wet-gets-wetter" mechanism in response to the mean warming, but dried by the "warmer-gets-wetter" mechanism because this region experiences a weaker warming than the rest of the tropics (i.e., a relative SST cooling). Based on a hierarchy of models, Widlansky et al. (2013) suggested that the diversity of precipitation responses simulated by CMIP models in this region is related to the amplitude of the mean warming. They hypothesized that the drying of the SPCZ in simulations with a modest warming (1°–2°C) was due to a dominant "warmer-gets-wetter" mechanism in that case, while the dominant "wet-gets-wetter" mechanism would lead to a rainfall increase in simulations with a stronger mean warming (>3°C). Our results based on idealized atmospheric experiments do not support this interpretation. The "wet-gets-wetter" mechanism only induces a very modest rainfall increase under the SPCZ under the ~3°C mean warming we consider, while the "warmer-gets-wetter" mechanism drives considerably

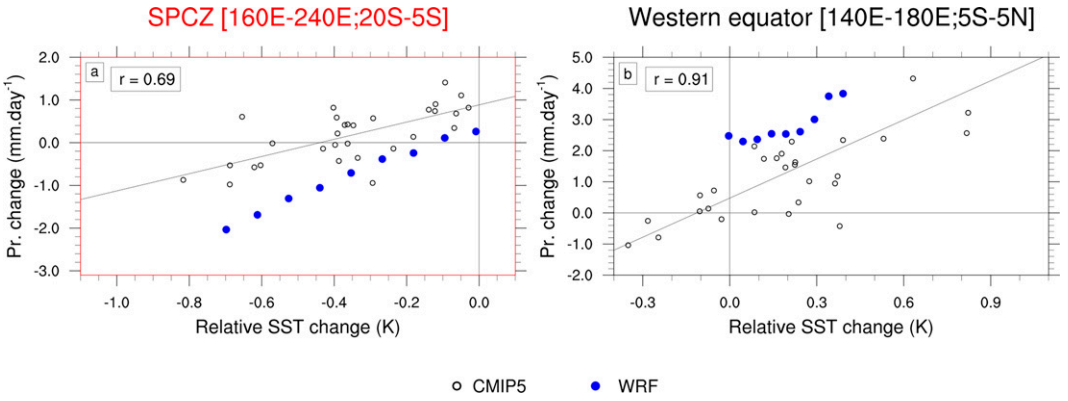

FIG. 9. Precipitation changes vs relative SST changes in CMIP5 models and ABSW experiment. Scatterplots of the average (a) SPCZ (20°–5°S, 160°–240°E) and (b) western equatorial Pacific (5°S–5°N, 140°–180°E) precipitation (mm day^{-1}) vs the average relative SST changes (in K). The black circles represent the CMIP5 models and the blue dots represent our simulations with WRF. The CMIP5 intermodel correlation coefficient (r) is indicated on the upper-left side of panels.

larger rainfall changes. In addition, our results show that precipitation changes are very sensitive to zonal SST gradient changes, while the enhanced equatorial warming plays a smaller role in this region (Fig. 8d).

Figure 9 examines whether this conclusion is also valid within the CMIP5 multimodel database. In the SPCZ region, there is a significant linear relationship (r = 0.69) between changes in relative SST and changes in precipitation simulated by CMIP5 models (Fig. 9a). Colder relative SST changes lead to a drier SPCZ, supporting a strong influence of the "warmer-gets-wetter" mechanism, in agreement with the results from our modeling framework. This relationship is also consistent with the key role played by dynamical processes in our results. The most striking difference on Fig. 9a is a −0.6 mm day^{-1} offset of our experiments relative to CMIP5, making the sign of the rainfall change much more consistent in our experimental set than in CMIP5 models. This difference could be due to a weaker wet-gets-wetter mechanism in our simulations than in CMIP5 models. The wet-gets-wetter mechanism is indeed stronger in presence of stronger background convection (Chou and Neelin 2004). As CMIP5 models tend to overestimate precipitation in the SPCZ core relative to observations and our simulations [e.g., Lintner et al. (2016) and Table 2], this may lead to an overestimated wet-gets-wetter mechanism in CMIP simulations than in our simulations. This also suggests that CMIP5 model inconsistencies in precipitation changes under SPCZ are partly related to their overestimation of climatological precipitation in this region. Another possible explanation is the lack of air-sea coupling which could exacerbate the precipitation response in our experimental setup. In coupled models, the drying in response to cold relative SST anomalies should indeed increase downward shortwave radiations and hence damp the initial cooling (e.g., Li et al. 2016; Ying et al. 2019), an effect that is not captured in our forced framework. The potential effects of other coupled feedbacks such as the Bjerknes feedback is more difficult to anticipate, and more studies will probably be needed in a coupled framework.

The relative SST changes from CMIP5 models are quite robust in the central and eastern equatorial Pacific (Fig. 1b). We will thus focus on the western Pacific box (Fig. 1b). In that region, CMIP5 relative SST and precipitation changes also exhibit a positive linear relationship (Fig. 9b, r = 0.91): more positive relative SST changes lead to a wetter western equatorial region. This relationship is similar in our simulations with a slope of 6 mm day^{-1} K^{-1}, although we note that we do not span the full range of relative SST changes in CMIP, because we do not vary the amplitude of the enhanced equatorial warming in our experimental framework. The offset between CMIP5 models and our simulations is also consistent with a different efficiency of the wet-gets-wetter (or dry-gets-drier at the equator) mechanism in our experiments and CMIP5 models, this time more underestimated in our simulations than in the CMIP5 models (but underestimated in both) due to a drier bias in the western equatorial region (Table 2). Despite this potential underestimation of the wet-gets-wetter mechanism in CMIP5 models, the strong correlation between the rainfall and SST changes is consistent with previous studies pointing to a dominant role of the warmer-gets-wetter mechanism in the western equatorial Pacific (e.g., Xie et al. 2010; Ma and Xie 2013). An additional result from our study is that this warmer-gets-wetter mechanism is boosted by nonlinear interactions between the equatorial enhanced warming and the zonal SST gradient changes for cases that correspond to a strong weakening of the zonal equatorial SST gradient.

One advantage of our model relative to CMIP5 models is the use of a pseudo–global warming approach which avoids the adverse effects of the large present-day SST biases in CMIP models. However, this comes also with uncertainties. While CMIP uses a variety of models, our results are from a single model, with some precipitation biases in CTRL such as the dry bias in the western equatorial Pacific (Fig. 2). Therefore, these results need to be extended to other models to be confirmed, with notably other parameterization of the convection which is an important source of uncertainty for the precipitation projections (e.g., Evans et al. 2016). Additionally, in our

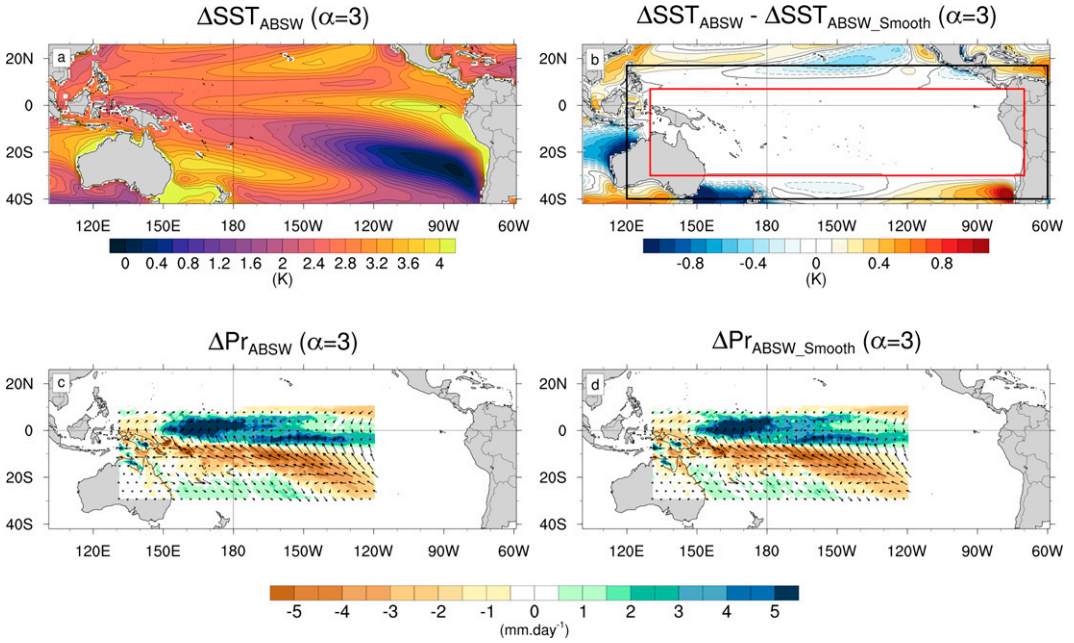

FIG. A1. (top) DJF climatology (in °C) of (a) ΔSST_{ABSW} (for $\alpha = 3$) and (b) difference between ΔSST_{ABSW} and ΔSST_{ABSW_Smooth}. The red box represents the area where $\Delta SST_{ABSW\_Smooth} = \Delta SST_{ABSW}$ (for $\alpha = 3$), the space between the black and red boxes represents the area where the smoothing is applied from ΔSST_{ABSW} (for $\alpha = 3$) to ΔSST_{ABSW} (for $\alpha = 1$), and outside of the black box $\Delta SST_{ABSW\_Smooth} = \Delta SST_{ABSW}$ (for $\alpha = 1$). (bottom) Averaged DJF precipitation (shading; in mm day^{-1}) and surface wind (vectors; in m s^{-1}) changes (relative to CTRL simulation) in (c) ABSW (for $\alpha = 3$) and in (d) ABSW_Smooth.

experimental strategy, the spatial pattern varies but not the amplitude of the mean forcing. There are however uncertainties in the latter, for instance associated with the future evolution of greenhouse gases concentrations. This should just add a constant offset to rainfall changes in the SPCZ region, but may modify the range of SST pattern changes for which nonlinearities operate in the equatorial region. Despite those uncertainties linked to our model and experimental framework, the comparison between our results and CMIP5 models discussed above suggests similar mechanisms in the two datasets.

The uncertainties associated to the zonal equatorial warming pattern has been statistically related to the intensity of the cold tongue bias (e.g., Li et al. 2015, 2016; Ying et al. 2019). The underpinning physical mechanism is that the cold tongue bias favors 1) a too-weak negative cloud-SST feedback in the western Pacific and 2) a too-strong wind-upwelling dynamic feedback in the eastern Pacific, inducing a westward shift of the warming pattern, i.e., a less "Niño-like," more "Niña-like" warming pattern. Our results highlight the importance of zonal SST gradient changes for future rainfall projections, especially under the SPCZ. Given the uncertainties in the spatial pattern of SST changes it is thus critical to better understand their cause and reduce their uncertainties for more robust estimates of future rainfall changes. Toward that goal, some emerging constraint methods have been developed to better constrain SST changes projected by CMIP models (Li et al. 2016). Such methods tend to lead to a larger reduction of the zonal equatorial SST gradient, similar to that imposed in our $\alpha = 2.5$ experiment (Fig. 1d). Dutheil et al. (2019) used such statistically corrected SST projections in a dynamical atmospheric downscaling exercise for the SPCZ region. This approach resulted in a much stronger SPCZ drying than in CMIP (−25% vs −7%). Similarly, the experimental setup used in that paper indicates a 1.7 mm day^{-1} (−30%) drying of the SPCZ for $\alpha = 2.5$. Both studies hence suggest that the future SPCZ may become much drier than what CMIP models currently project, however those studies do not explicitly account for the effect of air–sea coupling. In the future, it may hence be interesting to compare the impact of emergent constraint methods (statistical correction of projections based on present-day bias) to dynamical methods (where the present-day bias of a climate model is corrected, for instance via a flux correction approach) on future SST and rainfall changes. In addition, given that the El Niño–like response seems to be most robust in models (e.g., Li et al. 2016), it may also be advisable to select models in terms of their ability to reproduce the rainfall response to El Niño events over the historical period, in order to obtain a more robust estimate of the projected rainfall response. Finally, the spatial pattern of SST changes also has a remote influence on remote regional climate regimes, such as the Indian (e.g., Li et al. 2017) or North American (He et al. 2020) monsoons. A more robust estimate of the spatial pattern of tropical Pacific SST changes would hence also reduce projection uncertainties at a larger scale than indicated in this

study. These are among questions to be explored in the future.

Acknowledgments. CD was supported by the Leibniz Institute for Baltic Sea Research Warnemünde; ML, JV, and CM were supported by Institut de Recherche pour le Développement (IRD); and SW was supported by IFREMER. The authors acknowledge the Pôle de Calcul et de Données Marines (PCDM) for providing DATARMOR storage and computational resources (http://www.ifremer.fr/pcdm).

Data availability statement. The code and data used in this study are available under reasonable request.

APPENDIX

Sensitivity of Our Results to Lateral Boundary Conditions

Because variation of zonal asymmetry is applied all over the grid, it yields an inconsistency between the SST and the air temperature at the lateral boundaries (since the air temperature is kept constant for all α). This inconsistency is maximum for the simulations with $\alpha = 3$. Therefore, to evaluate the potential effects of these temperature inconsistencies at the boundaries, an additional simulation (called ABSW_smooth) has been performed where the modification of zonal asymmetry ($\alpha = 3$) is applied only in a central part of our domain, and the SST field smoothly transitioned to the CMIP5 MMM closer to the boundaries, avoiding the temperature lateral inconsistencies. The precipitation and wind surface changes relative to the CTRL run in ABSW_Smooth and ABSW are very similar (Fig. A1), highlighting that the inconsistency between SST and the lateral boundaries has only a minor impact on our results, probably since the boundaries are far from the studied areas.

REFERENCES

Adler, R. F., and Coauthors, 2003: The version-2 Global Precipitation Climatology Project (GPCP) Monthly Precipitation Analysis (1979–present). *J. Hydrometeor.*, **4**, 1147–1167, https://doi.org/10.1175/1525-7541(2003)004<1147:TVGPCP>2.0.CO;2.

Bretherton, C. S., and S. Park, 2009: A new moist turbulence parameterization in the Community Atmosphere Model. *J. Climate*, **22**, 3422–3448, https://doi.org/10.1175/2008JCLI2556.1.

Brown, J. R., A. F. Moise, and R. A. Colman, 2013: The South Pacific Convergence Zone in CMIP5 simulations of historical and future climate. *Climate Dyn.*, **41**, 2179–2197, https://doi.org/10.1007/s00382-012-1591-x.

——, and Coauthors, 2020: South Pacific Convergence Zone dynamics, variability and impacts in a changing climate. *Nat. Rev. Earth Environ.*, **1**, 530–543, https://doi.org/10.1038/s43017-020-0078-2.

Byrne, M. P., A. G. Pendergrass, A. D. Rapp, and K. R. Wodzicki, 2018: Response of the intertropical convergence zone to climate change: Location, width, and strength. *Curr. Climate Change Rep.*, **4**, 355–370, https://doi.org/10.1007/s40641-018-0110-5.

Cai, W., and Coauthors, 2019: Pantropical climate interactions. *Science*, **363**, eaav4236, https://doi.org/10.1126/science.aav4236.

——, and Coauthors, 2021: Changing El Niño–Southern Oscillation in a warming climate. *Nat. Rev. Earth Environ.*, **2**, 628–644, https://doi.org/10.1038/s43017-021-00199-z.

Chadwick, R., I. Boutle, and G. Martin, 2013: Spatial patterns of precipitation change in CMIP5: Why the rich do not get richer in the tropics. *J. Climate*, **26**, 3803–3822, https://doi.org/10.1175/JCLI-D-12-00543.1.

Chen, F., and J. Dudhia, 2001: Coupling an advanced land surface–hydrology model with the Penn State–NCAR MM5 modeling system. Part I: Model implementation and sensitivity. *Mon. Wea. Rev.*, **129**, 569–585, https://doi.org/10.1175/1520-0493(2001)129<0569:CAALSH>2.0.CO;2.

Chou, C., and J. D. Neelin, 2004: Mechanisms of global warming impacts on regional tropical precipitation. *J. Climate*, **17**, 2688–2701, https://doi.org/10.1175/1520-0442(2004)017<2688:MOGWIO>2.0.CO;2.

Chung, C. T. Y., S. B. Power, J. M. Arblaster, H. A. Rashid, and G. L. Roff, 2014: Nonlinear precipitation response to El Niño and global warming in the Indo-Pacific. *Climate Dyn.*, **42**, 1837–1856, https://doi.org/10.1007/s00382-013-1892-8.

Chung, E.-S., A. Timmermann, B. J. Soden, K.-J. Ha, L. Shi, and V. O. John, 2019: Reconciling opposing Walker circulation trends in observations and model projections. *Nat. Climate Change*, **9**, 405–412, https://doi.org/10.1038/s41558-019-0446-4.

Coats, S., and K. B. Karnauskas, 2017: Are simulated and observed twentieth century tropical Pacific sea surface temperature trends significant relative to internal variability? *Geophys. Res. Lett.*, **44**, 9928–9937, https://doi.org/10.1002/2017GL074622.

Collins, W. D., and Coauthors, 2004: Description of the NCAR Community Atmosphere Model (CAM 3.0). Tech. Rep. NCAR/TN-464+STR, University Corporation for Atmospheric Research, 226 pp., https://doi.org/10.5065/D63N21CH.

DiNezio, P. N., A. C. Clement, G. A. Vecchi, B. J. Soden, B. P. Kirtman, and S.-K. Lee, 2009: Climate response of the equatorial Pacific to global warming. *J. Climate*, **22**, 4873–4892, https://doi.org/10.1175/2009JCLI2982.1.

Duncan, D., 2012: Freshwater Under Threat: Pacific Islands: Vulnerability Assessment of Freshwater Resources of Environmental Change. Secretariat of the Pacific Community, Applied Geoscience and Technology Division, and United Nations Environment Programme, UNEP, 66 pp.

Dutheil, C., and Coauthors, 2019: Impact of surface temperature biases on climate change projections of the South Pacific Convergence Zone. *Climate Dyn.*, **53**, 3197–3219, https://doi.org/10.1007/s00382-019-04692-6.

——, and Coauthors, 2020: Impact of projected sea surface temperature biases on tropical cyclones projections in the South Pacific. *Sci. Rep.*, **10**, 4838, https://doi.org/10.1038/s41598-020-61570-6.

——, C. Menkes, M. Lengaigne, J. Vialard, A. Peltier, M. Bador, and X. Petit, 2021: Fine-scale rainfall over New Caledonia under climate change. *Climate Dyn.*, **56**, 87–108, https://doi.org/10.1007/s00382-020-05467-0.

Evans, J. P., K. Bormann, J. Katzfey, S. Dean, and R. Arritt, 2016: Regional climate model projections of the South Pacific Convergence Zone. *Climate Dyn.*, **47**, 817–829, https://doi.org/10.1007/s00382-015-2873-x.

Falkland, T., 2002: Volume 2: A synopsis of information relating to the quality of freshwater and watershed management issues in the Pacific Islands region. SPERP, 98 pp.

Flannaghan, T. J., S. Fueglistaler, I. M. Held, S. Po-Chedley, B. Wyman, and M. Zhao, 2014: Tropical temperature trends in Atmospheric General Circulation Model simulations and the impact of uncertainties in observed SSTs. *J. Geophys. Res. Atmos.*, **119**, 13 327–13 337, https://doi.org/10.1002/2014JD022365.

Fueglistaler, S., C. Radley, and I. M. Held, 2015: The distribution of precipitation and the spread in tropical upper tropospheric temperature trends in CMIP5/AMIP simulations. *Geophys. Res. Lett.*, **42**, 6000–6007, https://doi.org/10.1002/2015GL064966.

Graham, N. E., and T. P. Barnett, 1987: Sea surface temperature, surface wind divergence, and convection over tropical oceans. *Science*, **238**, 657–659, https://doi.org/10.1126/science.238.4827.657.

Grose, M. R., and Coauthors, 2014: Assessment of the CMIP5 global climate model simulations of the western tropical Pacific climate system and comparison to CMIP3. *Int. J. Climatol.*, **34**, 3382–3399, https://doi.org/10.1002/joc.3916.

Hall, A., P. Cox, C. Huntingford, and S. Klein, 2019: Progressing emergent constraints on future climate change. *Nat. Climate Change*, **9**, 269–278, https://doi.org/10.1038/s41558-019-0436-6.

He, C., T. Li, and W. Zhou, 2020: Drier North American monsoon in contrast to Asian–African monsoon under global warming. *J. Climate*, **33**, 9801–9816, https://doi.org/10.1175/JCLI-D-20-0189.1.

Held, I. M., and B. J. Soden, 2006: Robust responses of the hydrological cycle to global warming. *J. Climate*, **19**, 5686–5699, https://doi.org/10.1175/JCLI3990.1.

Izumo, T., J. Vialard, M. Lengaigne, and I. Suresh, 2020: Relevance of relative sea surface temperature for tropical rainfall interannual variability. *Geophys. Res. Lett.*, **47**, e2019GL086182, https://doi.org/10.1029/2019GL086182.

Johnson, N. C., and S.-P. Xie, 2010: Changes in the sea surface temperature threshold for tropical convection. *Nat. Geosci.*, **3**, 842–845, https://doi.org/10.1038/ngeo1008.

Li, G., and S.-P. Xie, 2014: Tropical biases in CMIP5 multimodel ensemble: The excessive equatorial Pacific cold tongue and double ITCZ problems. *J. Climate*, **27**, 1765–1780, https://doi.org/10.1175/JCLI-D-13-00337.1.

——, Y. Du, H. Xu, and B. Ren, 2015: An intermodel approach to identify the source of excessive equatorial Pacific cold tongue in CMIP5 models and uncertainty in observational datasets. *J. Climate*, **28**, 7630–7640, https://doi.org/10.1175/JCLI-D-15-0168.1.

——, S.-P. Xie, Y. Du, and Y. Luo, 2016: Effects of excessive equatorial cold tongue bias on the projections of tropical Pacific climate change. Part I: The warming pattern in CMIP5 multi-model ensemble. *Climate Dyn.*, **47**, 3817–3831, https://doi.org/10.1007/s00382-016-3043-5.

——, ——, C. He, and Z. Chen, 2017: Western Pacific emergent constraint lowers projected increase in Indian summer monsoon rainfall. *Nat. Climate Change*, **7**, 708–712, https://doi.org/10.1038/nclimate3387.

Lin, J.-L., 2007: The double-ITCZ problem in IPCC AR4 coupled GCMs: Ocean–atmosphere feedback analysis. *J. Climate*, **20**, 4497–4525, https://doi.org/10.1175/JCLI4272.1.

Lin, Y.-L., R. D. Farley, and H. D. Orville, 1983: Bulk parameterization of the snow field in a cloud model. *J. Climate Appl. Meteor.*, **22**, 1065–1092, https://doi.org/10.1175/1520-0450(1983)022<1065:BPOTSF>2.0.CO;2.

Lintner, B. R., B. Langenbrunner, J. D. Neelin, B. T. Anderson, M. J. Niznik, G. Li, and S.-P. Xie, 2016: Characterizing CMIP5 model spread in simulated rainfall in the Pacific Intertropical Convergence and South Pacific Convergence Zones. *J. Geophys. Res. Atmos.*, **121**, 11 590–11 607, https://doi.org/10.1002/2016JD025284.

Liu, Z., S. Vavrus, F. He, N. Wen, and Y. Zhong, 2005: Rethinking tropical ocean response to global warming: The enhanced equatorial warming. *J. Climate*, **18**, 4684–4700, https://doi.org/10.1175/JCLI3579.1.

Luo, J.-J., G. Wang, and D. Dommenget, 2018: May common model biases reduce CMIP5's ability to simulate the recent Pacific La Niña-like cooling? *Climate Dyn.*, **50**, 1335–1351, https://doi.org/10.1007/s00382-017-3688-8.

Ma, J., and S.-P. Xie, 2013: Regional patterns of sea surface temperature change: A source of uncertainty in future projections of precipitation and atmospheric circulation. *J. Climate*, **26**, 2482–2501, https://doi.org/10.1175/JCLI-D-12-00283.1.

McIver, L., and Coauthors, 2016: Health impacts of climate change in Pacific island countries: A regional assessment of vulnerabilities and adaptation priorities. *Environ. Health Perspect.*, **124**, 1707–1714, https://doi.org/10.1289/ehp.1509756.

Neelin, J. D., and I. M. Held, 1987: Modeling tropical convergence based on the moist static energy budget. *Mon. Wea. Rev.*, **115**, 3–12, https://doi.org/10.1175/1520-0493(1987)115<0003:MTCBOT>2.0.CO;2.

Power, S., and Coauthors, 2021: Decadal climate variability in the tropical Pacific: Characteristics, causes, predictability, and prospects. *Science*, **374**, eaay9165, https://doi.org/10.1126/science.aay9165.

Ramanathan, V., and W. Collins, 1991: Thermodynamic regulation of ocean warming by cirrus clouds deduced from observations of the 1987 El Niño. *Nature*, **351**, 27–32, https://doi.org/10.1038/351027a0.

Samanta, D., K. B. Karnauskas, and N. F. Goodkin, 2019: Tropical Pacific SST and ITCZ biases in climate models: Double trouble for future rainfall projections? *Geophys. Res. Lett.*, **46**, 2242–2252, https://doi.org/10.1029/2018GL081363.

Seager, R., N. Naik, and G. A. Vecchi, 2010: Thermodynamic and dynamic mechanisms for large-scale changes in the hydrological cycle in response to global warming. *J. Climate*, **23**, 4651–4668, https://doi.org/10.1175/2010JCLI3655.1.

——, M. Cane, N. Henderson, D.-E. Lee, R. Abernathey, and H. Zhang, 2019: Strengthening tropical Pacific zonal sea surface temperature gradient consistent with rising greenhouse gases. *Nat. Climate Change*, **9**, 517–522, https://doi.org/10.1038/s41558-019-0505-x.

Sobel, A. H., I. M. Held, and C. S. Bretherton, 2002: The ENSO signal in tropical tropospheric temperature. *J. Climate*, **15**, 2702–2706, https://doi.org/10.1175/1520-0442(2002)015<2702:TESITT>2.0.CO;2.

Taylor, K. E., R. J. Stouffer, and G. A. Meehl, 2012: An overview of CMIP5 and the experiment design. *Bull. Amer. Meteor. Soc.*, **93**, 485–498, https://doi.org/10.1175/BAMS-D-11-00094.1.

van der Wiel, K., A. J. Matthews, M. M. Joshi, and D. P. Stevens, 2016: Why the South Pacific Convergence Zone is diagonal. *Climate Dyn.*, **46**, 1683–1698, https://doi.org/10.1007/s00382-015-2668-0.

Watanabe, M., J.-L. Dufresne, Y. Kosaka, T. Mauritsen, and H. Tatebe, 2021: Enhanced warming constrained by past trends in equatorial Pacific sea surface temperature gradient. *Nat. Climate Change*, **11**, 33–37, https://doi.org/10.1038/s41558-020-00933-3.

Widlansky, M. J., A. Timmermann, K. Stein, S. McGregor, N. Schneider, M. H. England, M. Lengaigne, and W. Cai, 2013: Changes in South Pacific rainfall bands in a warming climate. *Nat. Climate Change*, **3**, 417–423, https://doi.org/10.1038/nclimate1726.

Xie, P., and P. A. Arkin, 1997: Global precipitation: A 17-year monthly analysis based on gauge observations, satellite estimates, and numerical model outputs. *Bull. Amer. Meteor. Soc.*, **78**, 2539–2558, https://doi.org/10.1175/1520-0477(1997)078<2539:GPAYMA>2.0.CO;2.

Xie, S.-P., C. Deser, G. A. Vecchi, J. Ma, H. Teng, and A. T. Wittenberg, 2010: Global warming pattern formation: Sea surface temperature and rainfall. *J. Climate*, **23**, 966–986, https://doi.org/10.1175/2009JCLI3329.1.

——, and Coauthors, 2015: Towards predictive understanding of regional climate change. *Nat. Climate Change*, **5**, 921–930, https://doi.org/10.1038/nclimate2689.

Ying, J., P. Huang, T. Lian, and H. Tan, 2019: Understanding the effect of an excessive cold tongue bias on projecting the tropical Pacific SST warming pattern in CMIP5 models. *Climate Dyn.*, **52**, 1805–1818, https://doi.org/10.1007/s00382-018-4219-y.

Zebiak, S. E., 1986: Atmospheric convergence feedback in a simple model for El Niño. *Mon. Wea. Rev.*, **114**, 1263–1271, https://doi.org/10.1175/1520-0493(1986)114<1263:ACFIAS>2.0.CO;2.

Zhang, G. J., and N. A. McFarlane, 1995: Sensitivity of climate simulations to the parameterization of cumulus convection in the Canadian Climate Centre general circulation model. *Atmos.–Ocean*, **33**, 407–446, https://doi.org/10.1080/07055900.1995.9649539.

Zhou, Z.-Q., and S.-P. Xie, 2015: Effects of climatological model biases on the projection of tropical climate change. *J. Climate*, **28**, 9909–9917, https://doi.org/10.1175/JCLI-D-15-0243.1.